nature communications

Article

https://doi.org/10.1038/s41467-024-52729-0

Metabolic regulation of cytoskeleton functions by HDAC6-catalyzed α-tubulin lactylation

Received: 14 March 2024

Accepted: 18 September 2024

Published online: 27 September 2024

Check for updates

Shuangshuang Sun[1,5], Zhe Xu[1,5], Liying He[1], Yihui Shen[1], Yuqing Yan[2], Xubing Lv[1], Xujing Zhu[1], Wei Li[1,3], Wei-Ya Tian[1], Yongjun Zheng[2], Sen Lin[4], Yadong Sun[1] & Lei Li[1,3]

Posttranslational modifications (PTMs) of tubulin, termed the "tubulin code", play important roles in regulating microtubule functions within subcellular compartments for specialized cellular activities. While numerous tubulin PTMs have been identified, a comprehensive understanding of the complete repertoire is still underway. In this study, we report that α-tubulin lactylation is catalyzed by HDAC6 by using lactate to increase microtubule dynamics in neurons. We identify lactylation on lysine 40 of α-tubulin in the soluble tubulin dimers. Notably, lactylated α-tubulin enhances microtubule dynamics and facilitates neurite outgrowth and branching in cultured hippocampal neurons. Moreover, we discover an unexpected function of HDAC6, acting as the primary lactyltransferase to catalyze α-tubulin lactylation. HDAC6-catalyzed lactylation is a reversible process, dependent on lactate concentrations. Intracellular lactate concentration triggers HDAC6 to lactylate α-tubulin, a process dependent on its deacetylase activity. Additionally, the lactyltransferase activity may be conserved in HDAC family proteins. Our study reveals the primary role of HDAC6 in regulating α-tubulin lactylation, establishing a link between cell metabolism and cytoskeleton functions.

Microtubules, a major component of cytoskeletons are comprised of α/β-tubulin heterodimers that form a tubular structure in eukaryotic cells. Microtubules are highly dynamic and constantly undergo polymerization and depolymerization to perform their diverse functions, including intracellular transport, cell division, and cell migration[1,2]. For example, during neurite growth, dynamic microtubules within the growth cone facilitate the growth of new neurites, while stable microtubules in neurite shafts serve as the structural framework, supporting axonal transport and neurite elongation[3,4]. Posttranslational modifications (PTMs) of tubulin subunits, enriched in specialized microtubule structures, regulate microtubule dynamics at these specific sites[5,6]. The majority of these PTMs occur on the exterior of microtubules, but acetylation on α-tubulin Lys40 (K40) is found in the microtubule lumen to mark stable microtubules, particularly in cilia, flagella, and long-lived cytoplasmic microtubules with slow dynamics[7–9]. Stabilization of cellular microtubules by Taxol or microtubule-associated proteins (MAPs) increases α-tubulin acetylation[9,10]. Moreover, structural studies have revealed that α-tubulin acetylation may impair the lateral interaction among the protofilaments and increase microtubule stability during mechanical aging[11,12].

Acetylation of α-tubulin is regulated by the acetyltransferase MEC-17/α-TAT1 and the deacetylase HDAC6 or Sirt2[13–15]. α-Tubulin acetylation serves as the stable microtubule marker, probably results from the distinct preference of MEC-17 and HDAC6 for microtubule and tubulin heterodimers, respectively[16,17]. Moreover, α-tubulin acetylation

[1]School of Life Science and Technology, ShanghaiTech University, Shanghai, China. [2]Department of Pain management, HuaDong Hospital Affiliated to Fudan University, Shanghai, China. [3]Shanghai Clinical Research and Trial Center, Shanghai, China. [4]Department of Neurology, 2nd Affiliated Hospital, Army Medical University, Chongqing, China. [5]These authors contributed equally: Shuangshuang Sun, Zhe Xu. e-mail: lilei@shanghaitech.edu.cn

enhances the binding of motor proteins and plays an important role in early polarization events in neurons[18,19]. Deficiency of α-tubulin acetylation is related to impaired axonal transport[19,20], neuronal migration[21], and axonal growth[22]. Furthermore, α-tubulin acetylation may also play roles in neurodegenerative disorders, including Huntington's disease, Parkinson's disease, and Charcot-Marie-Tooth disease[20,23,24]. Moreover, α-tubulin K40 undergoes trimethylation to regulate cell division and neuronal migration during cortical development[25,26]. Although many PTMs of microtubules have been identified, there remains a need for further exploration to uncover the new PTMs of microtubules.

Recent studies have discovered a post-translational modification named protein lactylation, targeting lysine residues in both histones and non-histone proteins[27–30]. Acetyltransferases such as p300 or TIP60 have been shown to lactylate proteins by using lactyl-coenzyme A (Lac-CoA) as donor[27,31,32]. Additionally, HDAC proteins and Sirtuins have been found to remove protein lactylation[29,32–34]. Moreover, hypoxia and increased glycolysis have been demonstrated to elevate protein lactylation levels in various cell types[27,35,36]. However, the regulation mechanism of protein lactylation remains unclear.

In this study, we identify lactylation on K40 of α-tubulin, competing the same residue with acetylation. α-Tubulin lactylation distributes in the soluble tubulin dimers and increases microtubule dynamics. Interestingly, the α-tubulin deacetylase HDAC6 plays a primary role in regulating α-tubulin lactylation through directly lactylating α-tubulin in high lactate concentration. Finally, α-tubulin lactylation may enhance neurite outgrowth and branching in cultured neurons. Our study identifies α-tubulin lactylation, competing with acetylation in regulating microtubule dynamics, which links cell metabolism and cytoskeleton functions.

Results

Identification of α-tubulin lactylation on K40

To analyze lactylated proteins in cortical neurons, we extracted proteins from cultured neurons and digested them into peptides by trypsin. The lactylated peptides were purified using an anti-lysine lactylation (lac-K) antibody[27], and lysine lactylation was identified through high-performance liquid chromatography (HPLC)-tandem mass spectrometry (MS/MS) analysis (Fig. 1a). The standard for lysine lactylation identification was a mass shift of 72.021 Da on the lysine residue, indicative of the addition of a lactyl group. The mass spectrometry results revealed that 285 peptides had been modified by lactylation (Supplementary Data 1). These lactylated proteins are involved in various biological processes, including transcriptional regulation and cytoskeleton organization (Fig. 1b). Previous studies have investigated the lactylation regulation of histones and metabolic enzymes[27,37,38]. Our specific focus was on investigating lactylation on microtubules and microtubule-associated proteins, particularly α-tubulin.

The mass shift of 72.021 Da on the lysine residue in the peptide (HGIQPDGQMPSDKTIG) from α-tubulin and the cyclic immonium (CycIm) ion of lactyllysine formed during tandem mass spectrum[39] were identified through mass spectrometry analysis (Fig. 1c), suggesting α-tubulin may undergo lactylation on Lys40 (K40). To further validate lactylation of α-tubulin, we transfected HEK293T cells with HA-tagged α-tubulins encoded by different α-tubulin genes. Subsequently, the α-tubulins were immunoprecipitated, and lysine lactylation was revealed by the anti-Lac-K antibody. The immunoblot results revealed lactylation in α-tubulins encoded by *TUBA1A*, *TUBA1C*, *TUBA3B*, and *TUBA4A*. However, both lactylation and acetylation were absent in the α-tubulin encoded by *TUBA8* (Fig. 1d, e), probably due to the lack of K40 in *TUBA8*-encoded α-tubulin (Fig. 1d, e). We then generated a lysine to alanine mutation on the K40 residue of *TUBA1A*-encoded α-tubulin (α-tubulin^{K40A}) and found that lactylation was abolished in the mutant α-tubulin (Fig. 1f, g). Together, these results indicate that K40 is the major lactylation site of α-tubulin.

HDAC6 functions as a primary lactyltransferase for α-tubulin lactylation

Previous studies have indicated that acetyltransferases may also catalyze protein lactylation[27,29,32]. To identify the protein responsible for α-tubulin lactylation, we transfected various acetyltransferases into HEK293T cells and assessed α-tubulin lactylation levels. As expected, overexpression of the α-tubulin acetyltransferase MEC-17 led to a significant increase in α-tubulin lactylation (Supplementary Fig. 1a, b), suggesting that MEC-17 may function as an α-tubulin lactyltransferase. This lactylation was specifically on the K40 residue, as demonstrated by the abolition of α-tubulin lactylation in the α-tubulin^{K40A} mutant (Supplementary Fig. 1c, d). We next conducted an in vitro lactylation assay using GST-MEC-17 protein purified from *E. coli* and tubulins purified from the mouse brain. In the presence of Lac-CoA, MEC-17 catalyzed α-tubulin lactylation in a dose-dependent manner (Supplementary Fig. 1e, f). Interestingly, MEC-17 exhibited a preference for microtubules over tubulin dimers in catalyzing α-tubulin lactylation (Supplementary Fig. 1g, h), similar to its catalytic preference as acetyltransferase.

We next generated a polyclonal antibody against lactylated K40 peptide of α-tubulin by using the peptide containing lactylated K40 (Supplementary Fig. 2a). The antibody underwent negative screening with acetylated and un-modified peptides to eliminate nonspecific binding (Supplementary Fig. 2b) and exhibited no detectable cross-reactivity with acetylated or un-modified K40 peptides (Supplementary Fig. 2c). It specifically recognized lactylated α-tubulin in HEK293T cells, but not the α-tubulin^{K40A} mutant (Supplementary Fig. 2d). Taking advantage of this antibody, we compared α-tubulin lactylation levels in wildtype (WT) and MEC-17 knockout (KO) HEK293T cells. Despite the complete loss of α-tubulin acetylation, there was a slight and statistically nonsignificant reduction in α-tubulin lactylation in MEC-17-deficient cells (Supplementary Fig. 1i, j). These results suggest that α-tubulin acetyltransferase MEC-17 plays a minor role in regulating α-tubulin lactylation in cells.

Intriguingly, when we expressed HDAC family proteins in HEK293T cells, none of the HDACs exhibited delactylase activity for α-tubulin; however, HDAC6 overexpression significantly increased α-tubulin lactylation (Fig. 2a, b). Consistently, HDAC6 KO mice showed a substantial reduction in α-tubulin lactylation in the cortex (Fig. 2c, d). HDAC6-induced α-tubulin lactylation occurred on K40 residue, as the α-tubulin^{K40A} mutant abolished HDAC6's effect (Fig. 2e, f). Given that HDAC6 is known as an α-tubulin deacetylase, it is possible that HDAC6-induced α-tubulin lactylation results from reduced α-tubulin acetylation, making K40 available for lactylation. However, HDAC6 overexpression in MEC-17 KO cells, lacking α-tubulin acetylation, still increased α-tubulin lactylation (Fig. 2g, h), suggesting HDAC6 causes α-tubulin lactylation independently of α-tubulin acetylation.

To compare the contribution of MEC-17 and HDAC6 to α-tubulin lactylation, we generated MEC-17 KO, HDAC6 KO and MEC-17, HDAC6 double KO (dKO) mice. Analysis of α-tubulin lactylation levels in the cortex revealed a reduction in MEC-17 KO cortex compared to WT cortex (Fig. 2i, j). Furthermore, α-tubulin lactylation was further decreased in HDAC6 KO cortex compared with MEC-17 KO cortex, indicating that HDAC6 plays a major role in regulating α-tubulin lactylation. Intriguingly, α-tubulin lactylation was completely undetectable in MEC-17 and HDAC6 double KO cortex (Fig. 2i, j). These results indicate that both MEC-17 and HDAC6 contribute to α-tubulin lactylation with HDAC6 potentially acting as the primary lactyltransferase for α-tubulin lactylation.

HDAC6 catalyzes α-tubulin lactylation through a reversible reaction dependent on lactate concentration

While HDAC family proteins have been shown to remove protein lactylation to form lactate in the in vitro assay[33], HDAC6 overexpression led to increased α-tubulin lactylation (Fig. 2a). Considering the relative

https://doi.org/10.1038/s41467-024-52729-0

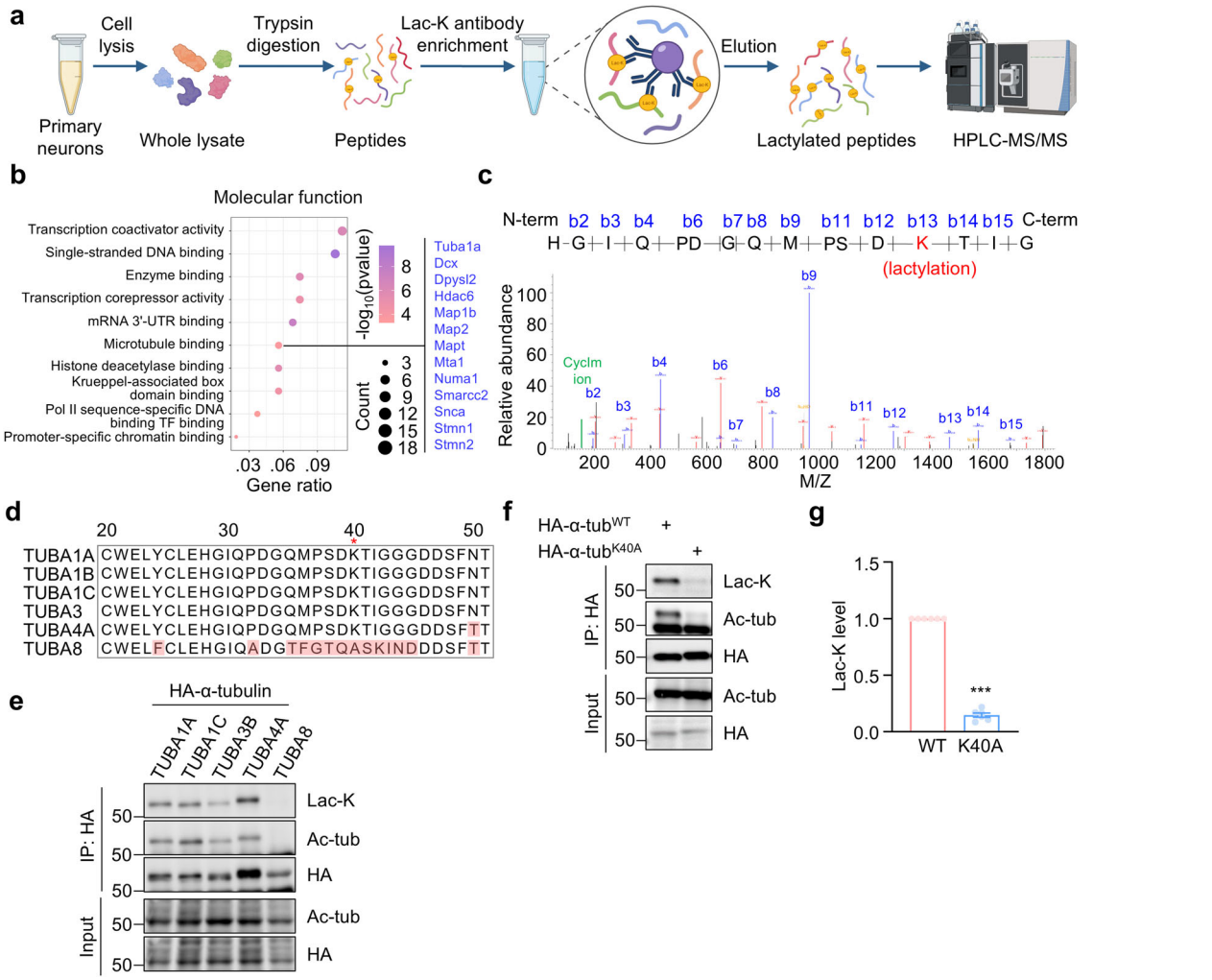

Fig. 1 | Identification of α-tubulin lactylation on K40. a Schematic diagram of purification and proteomic analysis of lactylated peptides from cultured neurons. **b** Top 10 significantly enriched molecular function of lactylated proteins. Two-sided Fisher's Exact Test, $p < 0.05$. **c** Mass spectrometry analysis showing lactylation at K40 on α-tubulin from cultured cortical neurons. Expected molecular weights of lactylated peptides from N terminus and C terminus are shown as peaks in red and blue, respectively. The CycIm ion at m/z 156.103 is shown as a peak in green. **d** Shown are amino acid sequences of tubulins encoded by different genes, including *TUBA1A*, *TUBA1B*, *TUBA1C*, *TUBA3*, *TUBA4A*, and *TUBA8*. The variant amino acids are indicated in red. **e** Lactylation of α-tubulin encoded by different genes. HEK293T cells were transfected with HA-tagged α-tubulins encoded by indicated tubulin genes. HA-α-tubulin was purified by immunoprecipitation with anti-HA antibody and α-tubulin lactylation was revealed by anti-Lac-K antibody. n = 3 experiments. **f** Abolished α-tubulin lactylation in K40A mutant. HEK293T cells were transfected with HA-tagged α-tubulin or α-tubulin K40A mutant. **g** Quantification analysis of data in (**f**). n = 6 experiments. Two-sided paired student's *t*-test, $p < 0.0001$. Data are shown as mean ± SEM. ***$p < 0.001$. Source data are provided as a Source Data file.

high lactate concentration (range from about 2 to 30 mM) in cells[40–42], we speculated that HDAC6-catalyzed α-tubulin delactylation is a reversible reaction and intracellular lactate concentration may trigger this reaction from delactylation to lactylation. To test this, we purified Flag-HDAC6 and incubated Flag-HDAC6 with tubulins in the presence of various lactate concentrations. HDAC6 displayed the delactylase activity at lactate concentrations below 1 mM but promoted α-tubulin lactylation at concentrations above 1 mM (Fig. 3a, b). Moreover, HDAC6 dose-dependently catalyzed α-tubulin lactylation in the presence of 10 mM lactate (Fig. 3c, d). We also measured the K_m of HDAC6 for lactate in catalyzing α-tubulin lactylation was 10.312 ± 4.421 mM, and the turnover number (K_{cat}) of HDAC6 was 0.006 ± 0.003 s^{-1} (Fig. 3e). Additionally, HDAC6 shows a preference for tubulin dimers over microtubules (Fig. 3f, g). These results demonstrate that HDAC6 lactylates α-tubulin through a reversible reaction dependent on lactate concentration.

The deacetylase activity of HDAC6 is critical for its lactylation activity

To determine whether HDAC6 deacetylase activity is required for lactylation, we applied HDAC inhibitors to impair the deacetylase activity. The HDAC inhibitor TSA effectively abolished HDAC6 catalytic activity for α-tubulin lactylation in the in vitro assay (Fig. 3h, i). Furthermore, HDAC6-induced α-tubulin lactylation was attenuated in cells treated with TSA or the HDAC6 inhibitor Tubastatin (TST) (Fig. 3j, k). HDAC6 contains two deacetylase domains, with the second deacetylase domain being crucial for α-tubulin deacetylation[43]. We generated mutations in two critical residues for deacetylase activity, Histidine (H)216 and H611, within the first and second deacetylase domain, respectively. Mutation of H611 but not H216 disrupted the lactylation activity for α-tubulin (Fig. 3l, m). These results indicate that HDAC6 deacetylase activity is crucial for its lactylation activity.

https://doi.org/10.1038/s41467-024-52729-0

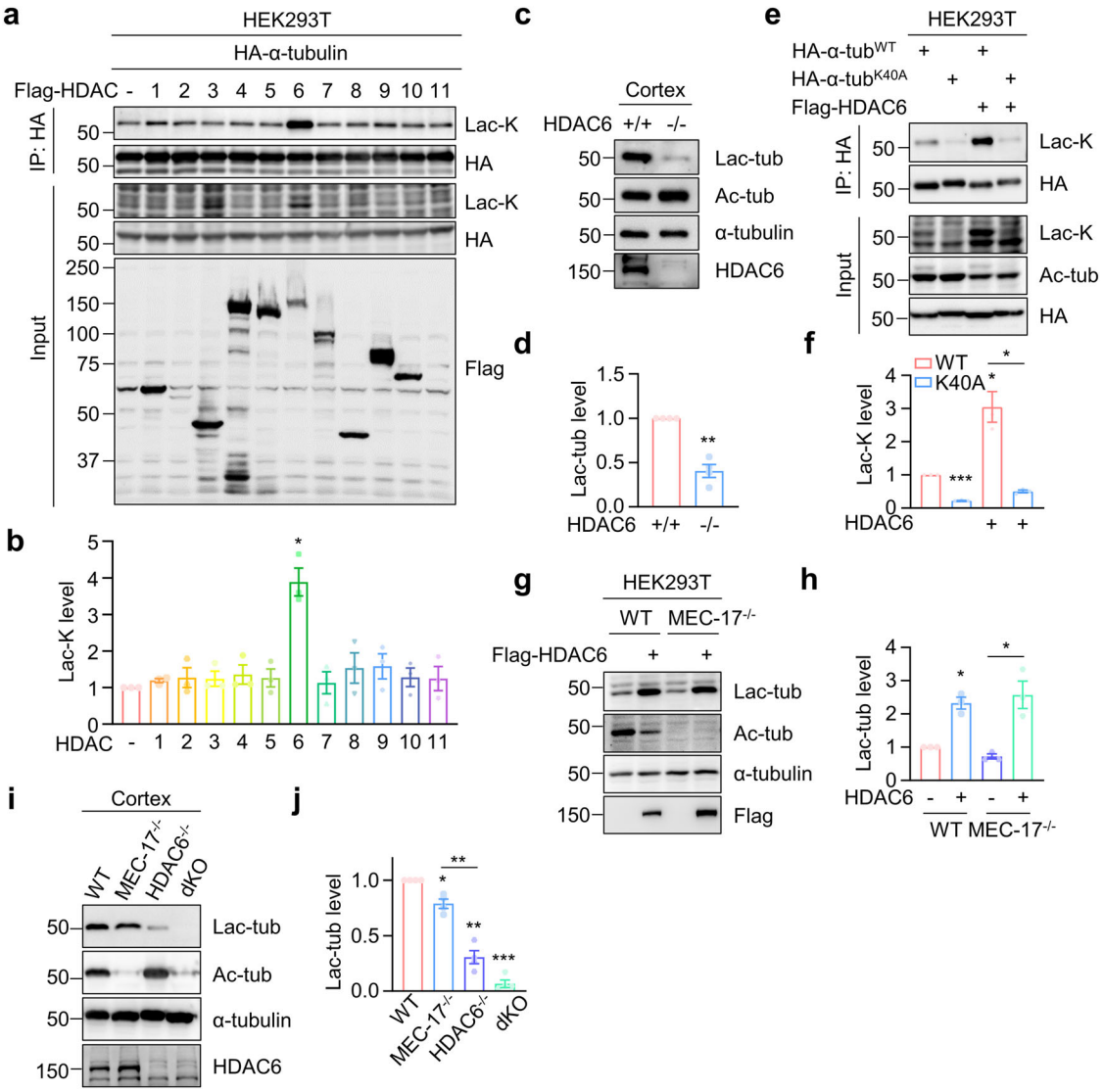

Fig. 2 | Identification of HDAC6 as a primary lactyltransferase for α-tubulin lactylation. a, **b** HDAC6 overexpression leads to increased α-tubulin lactylation. HEK293T cells were transfected with Flag-tagged HDAC family proteins, together with HA-α-tubulin. HA-α-tubulin was immunoprecipitated with anti-HA antibody and α-tubulin lactylation was revealed by anti-Lac-K antibody. n = 3 experiments. Two-sided paired student's *t*-test, HDAC6 vs control, p = 0.0170. **c**, **d** α-Tubulin lactylation is largely reduced in HDAC6-deficient cortex. n = 4 experiments. Two-sided paired student's *t*-test, HDAC6$^{-/-}$ vs HDAC6$^{+/+}$, p = 0.0038. **e**, **f** HDAC6-induced α-tubulin lactylation occurs on K40 residue. n = 3 experiments. Two-sided paired student's *t*-test, K40A vs WT, p = 0.0001; WT + HDAC6 vs WT, p = 0.0473; K40A + HDAC6 vs WT + HDAC6, p = 0.0369. **g**, **h** HDAC6-induced α-tubulin lactylation is independent of α-tubulin acetylation. n = 3 experiments. Two-sided paired student's *t*-test, WT + HDAC6 vs WT, p = 0.0171; MEC-17$^{-/-}$ + HDAC6 vs MEC-17$^{-/-}$, p = 0.0326. **i**, **j** HDAC6 plays the primary role in regulating α-tubulin lactylation. n = 4 experiments. Two-sided paired student's *t*-test, MEC-17$^{-/-}$ vs WT, p = 0.0146; HDAC6$^{-/-}$ vs WT, p = 0.0014; dKO vs WT, p = 0.0001; HDAC6$^{-/-}$ vs MEC-17$^{-/-}$, p = 0.0055. Data are shown as mean ± SEM. *p < 0.05, **p < 0.01, ***p < 0.001. Source data are provided as a Source Data file.

HDAC6 is required for metabolic regulation of α-tubulin lactylation

Given that high lactate concentration triggers HDAC6 to lactylate α-tubulin, the glycolysis pathway, which produces lactate, may increase α-tubulin lactylation. Indeed, HEK293T cells treated with various concentrations of lactate showed a dose-dependent induction of α-tubulin lactylation (Supplementary Fig. 3a, b), consistent with previous reports indicating that lactate enhances protein lactylation[27,32,35,44]. Similarly, GSKA, an inhibitor of lactate dehydrogenase (LDH) designed to prevent lactate production, reduced α-tubulin lactylation (Supplementary Fig. 3c, d). Next, HEK293T cells were exposed to various concentrations of glucose exhibited a dose-dependent increase in α-tubulin lactylation levels (Supplementary Fig. 3e, f). Conversely, the non-metabolizable glucose analog 2-deoxy-D-glucose (2-DG), which inhibits glycolysis, decreased α-tubulin lactylation levels (Supplementary Fig. 3g, h), indicating that glycolysis increases α-tubulin lactylation. Intracellular glucose metabolism is balanced by glycolysis and mitochondrial metabolism[45,46]. We treated HEK293T cells with rotenone, an inhibitor of mitochondrial respiratory chain complex I, to enhance glycolysis. Immunoblot revealed that rotenone treatment increased α-tubulin lactylation levels (Supplementary Fig. 3i, j). In the hypoxia conditions, the glycolysis is highly enhanced. We thus incubated the cells in 1% O_2 condition for 24 h, and found that global protein lactylation and α-tubulin lactylation were largely increased in cells after hypoxia (Supplementary Fig. 3k, l). In contrast, glucose depletion resulted in reduced global protein lactylation and α-tubulin lactylation (Supplementary Fig. 3m, n). These results demonstrate that

https://doi.org/10.1038/s41467-024-52729-0

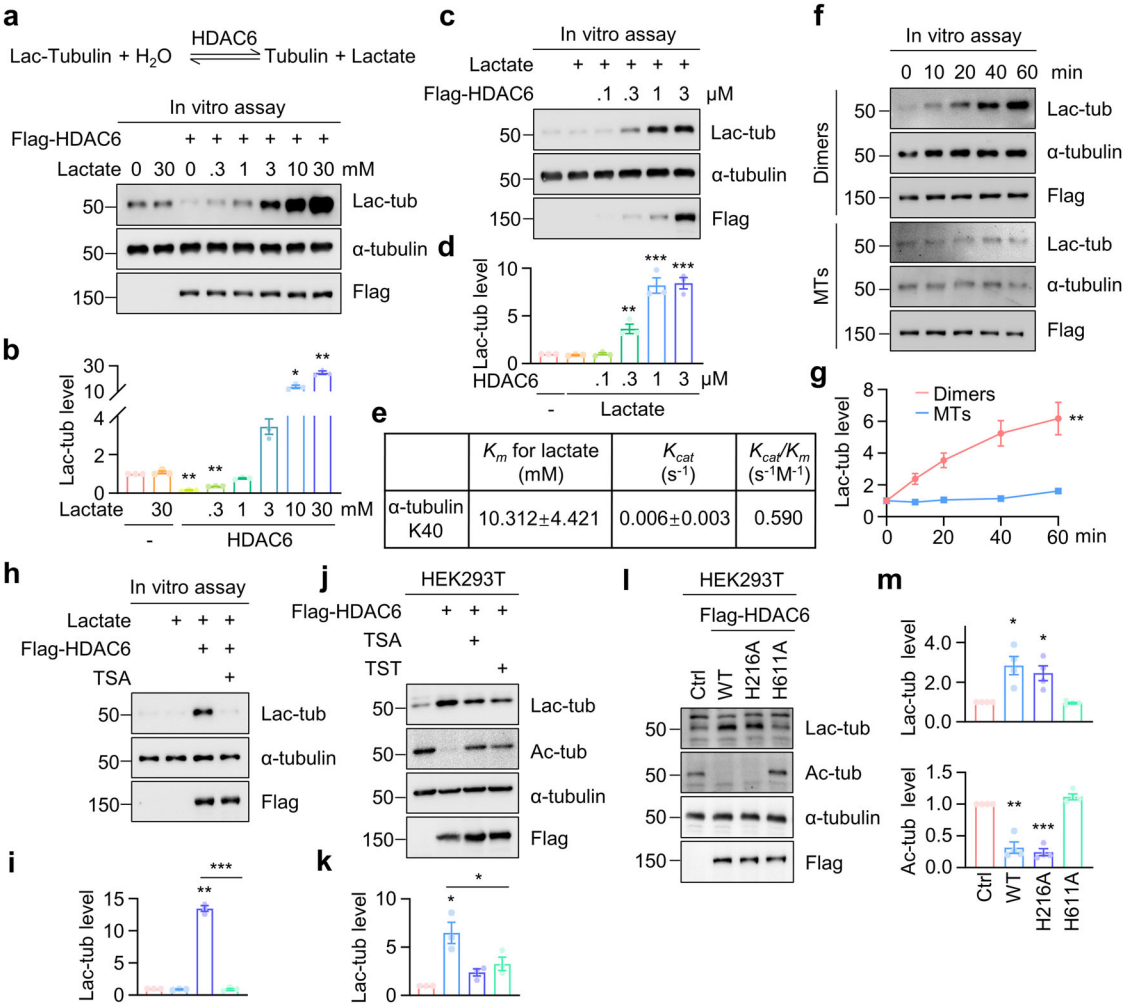

Fig. 3 | HDAC6 catalyzes α-tubulin lactylation through a reversible reaction dependent on its deacetylase activity. a, **b** In vitro assays using purified HDAC6 and tubulins in the presence of various concentrations of lactate. 4 μM Flag-HDAC6 and 2 μM tubulin dimers were incubated in the lactylation buffer with the indicated concentrations of lactate at 37 °C for 1 h, and α-tubulin lactylation was revealed by immunoblot. n = 3 experiments. One-way ANOVA, HDAC6 vs control, p = 0.0022; HDAC6 + 0.3 mM Lactate vs control, p = 0.0013; HDAC6 + 10 mM Lactate vs control, p = 0.0286; HDAC6 + 30 mM Lactate vs control, p = 0.0083. **c**, **d** HDAC6 catalyzes α-tubulin lactylation in a dose-dependent manner in the in vitro assay. The tubulin dimers at 2 μM and lactate at 10 mM were incubated with the indicated concentrations of Flag-HDAC6 at 37 °C for 1 h. n = 3 experiments. One-way ANOVA, Lactate + 0.3 μM HDAC6 vs control, p = 0.0061; Lactate + 1 μM HDAC6 vs control, p < 0.0001; Lactate + 3 μM HDAC6 vs control, p < 0.0001. **e** The K_m and K_{cat} of recombinant Flag-HDAC6 toward lactate were determined in the in vitro assay. **f**, **g** The catalytic preference of HDAC6 for tubulin dimers over microtubules (MTs) in the in vitro assay. 4 μM Flag-HDAC6 was incubated with 10 mM lactate, and 2 μM tubulin dimers or microtubules at 37 °C for the indicated time points. n = 3 experiments. Two-way ANOVA, Dimers vs MTs, p = 0.0057. **h**, **i** HDAC inhibitor TSA disrupts HDAC6 catalytic activity for α-tubulin lactylation in the in vitro assay. The in vitro assay was performed in the presence of 10 μM TSA. n = 3 experiments. Two-sided paired student's *t*-test, HDAC6 + Lactate vs control, p = 0.0012; HDAC6 + Lactate + TSA vs HDAC6 + Lactate, p = 0.0005. **j**, **k** HDAC inhibitor TSA and HDAC6 inhibitor TST attenuates HDAC6-induced α-tubulin lactylation in HEK293T cells. Cells were treated with 2 μM TSA or 2 μM TST for 20 h. n = 3 experiments. Two-sided paired student's *t*-test, HDAC6 vs control, p = 0.0386; HDAC6 + TSA vs HDAC6, p = 0.0718; HDAC6 + TST vs HDAC6, p = 0.0160. **l**, **m** HDAC6-catalyzed α-tubulin lactylation requires its deacetylase activity. n = 4 experiments. Two-sided paired student's *t*-test, for Lac-tub, WT vs Ctrl, p = 0.0279; H216A vs Ctrl, p = 0.0299. For Ac-tub, WT vs Ctrl, p = 0.0045; H216A vs Ctrl, p = 0.0008. Data are shown as mean ± SEM. *p < 0.05, **p < 0.01, ***p < 0.001. Source data are provided as a Source Data file.

α-tubulin lactylation is regulated by glycose metabolism, particularly glycolysis.

To determine whether lactate-induced α-tubulin lactylation is dependent on HDAC6, we generated HDAC6 KO HEK293T cells and treated the cells with lactate. Immunoblot revealed that lactate-induced α-tubulin lactylation was abolished in HDAC6-deficient cells (Supplementary Fig. 3o, p), suggesting the requirement of HDAC6 in lactate-induced α-tubulin lactylation. Furthermore, HDAC6-induced α-tubulin lactylation was significantly reduced with the LDH inhibitor GSKA treatment (Supplementary Fig. 3q, r). Together, these results indicate that glycolysis modulates α-tubulin lactylation through HDAC6-catalyzed lactylation reaction.

Sirt2 is an α-tubulin delactylase

Sirtuin family proteins have been shown to remove protein lactylation[32,34]. Subsequently, we screened the Sirtuin family proteins and observed that overexpression of Sirt2 resulted in decreased α-tubulin lactylation (Supplementary Fig. 4a, b). To further validate Sirt2 as an α-tubulin delactylase, we conducted an in vitro assay. The purified GST-Sirt2 catalyzed α-tubulin delactylation in a dose-dependent manner, and Sirt2 delactylase activity was found to be dependent on NAD+ (Supplementary Fig. 4c, d). Consistently, α-tubulin lactylation levels increased in Sirt2-deficient cells (Supplementary Fig. 4e, f), indicating that Sirt2 serves as an α-tubulin delactylase in vivo. Moreover, the in vitro assay revealed a significant reduction in α-tubulin

https://doi.org/10.1038/s41467-024-52729-0

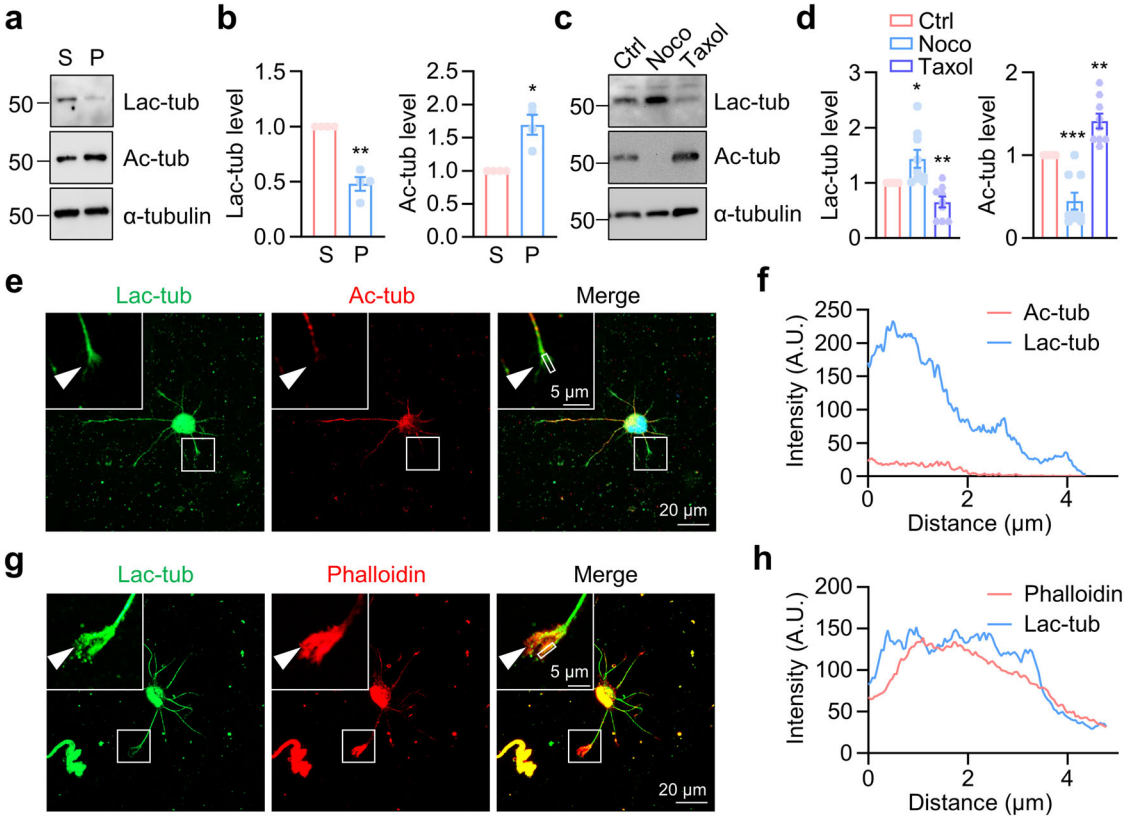

Fig. 4 | Distribution of lactylated α-tubulin in tubulin dimers. a, **b** Distribution of lactylated α-tubulin in the soluble tubulin dimers (S), but not the polymerized microtubules (P). n = 4 experiments. Two-sided paired student's *t*-test, for Lac-tub, p = 0.0037. For Ac-tub, p = 0.0193. **c**, **d** HEK293T cells were treated with Nocodazole (Noco) or Taxol for 12 h. Immunoblotting revealed α-tubulin lactylation levels in HEK293T cells after treatment. The concentration of Nocodazole or Taxol was 1 μM. n = 9 experiments. Two-sided paired student's *t*-test, for Lac-tub, Noco vs Ctrl, p = 0.0272; Taxol vs Ctrl, p = 0.0078. For Ac-tub, Noco vs Ctrl, p = 0.0006; Taxol vs Ctrl, p = 0.0018. **e**–**h** Representative images of cortical neurons at DIV1, stained using anti-lactylated-α-tubulin (green), and anti-acetylated-α-tubulin (red) in (**e**), and Phalloidin (red) to label F-actin in (**g**). The top left region indicates higher-magnification images. The arrow head indicates the growth cone. The fluorescence-intensity profile of lactylated-α-tubulin (blue), and acetylated-α-tubulin (red) in (**f**), or lactylated-α-tubulin (blue), and Phalloidin (red) in (**h**) were obtained along the while line. Data are shown as mean ± SEM. *p < 0.05, **p < 0.01, ***p < 0.001. Source data are provided as a Source Data file.

lactylation levels when Sirt2 was incubated with microtubules rather than tubulin dimers (Supplementary Fig. 4g, h), suggesting that Sirt2 catalyzes α-tubulin delactylation with the preference for microtubules.

Localization of lactylated α-tubulin in soluble tubulin dimers

Microtubules undergo dynamic polymerization and depolymerization, and tubulins may exist in polymerized microtubules or as soluble tubulin dimers[1,2]. To determine the localization of lactylated α-tubulin, we separated soluble tubulin dimers (S) and polymerized microtubules (P) in HEK293T cells. The results revealed that lactylated α-tubulin was predominantly present in the soluble fraction (Fig. 4a, b), probably resulting from the catalytic preference of HDAC6 for tubulin dimers. In contrast, acetylated α-tubulin was found in polymerized microtubules, as previously reported[8,9]. We next used microtubule-targeting agents to manipulate the balance between tubulin dimers and polymerized microtubules. Nocodazole (Noco), an inhibitor of microtubule assembly, resulted in reduced α-tubulin acetylation and increased α-tubulin lactylation (Fig. 4c, d). Conversely, Taxol, which stabilizes microtubules, led to increased α-tubulin acetylation and decreased α-tubulin lactylation (Fig. 4c, d). These findings indicate that α-tubulin lactylation marks soluble tubulin dimers, while acetylation on the same residue marks stable microtubules. Immunostaining using the anti-lactylated α-tubulin antibody was performed to examine the spatial distribution of lactylated α-tubulin in cultured hippocampal neurons. Lactylated α-tubulin was notably presented in the growth cone (Fig. 4e–h), where dynamic microtubules were enriched for neurite extension. In contrast, acetylated α-tubulin accumulated in the neurite shaft rather than the growth cone (Fig. 4e, f).

Increased microtubule dynamics by α-tubulin lactylation

To determine whether lactylated α-tubulin modulates microtubule dynamics, we purified microtubules from mouse brains and conducted the in vitro lactylation assay to obtain highly lactylated α-tubulin (Supplementary Fig. 5a–c). Microtubule formation is proposed to involve two key steps: tubulin nucleation and microtubule elongation[47,48]. In the analysis of tubulin nucleation, an early step in generating short microtubule seeds for assembly[11], we observed a significant increase in the number of short microtubules in chambers incubated with lactylated α-tubulin compared to native α-tubulin (Fig. 5a, b), suggesting α-tubulin lactylation enhances the tubulin nucleation process.

We next performed the in vitro microtubule reconstitution assay (Supplementary Fig. 5d) to assess the impact of α-tubulin lactylation on microtubule elongation. The time-lapse total internal reflection fluorescence (TIRF) imaging revealed a significant increase in both the growth rate and shrinkage rate, without a notable alteration in catastrophe frequency (Fig. 5c–f), These changes resulted in an increased maximum microtubule length in the chamber incubated with lactylated α-tubulin (Fig. 5g). Taken together, these results indicate that lactylated α-tubulin promotes tubulin nucleation and enhances microtubule dynamics.

https://doi.org/10.1038/s41467-024-52729-0

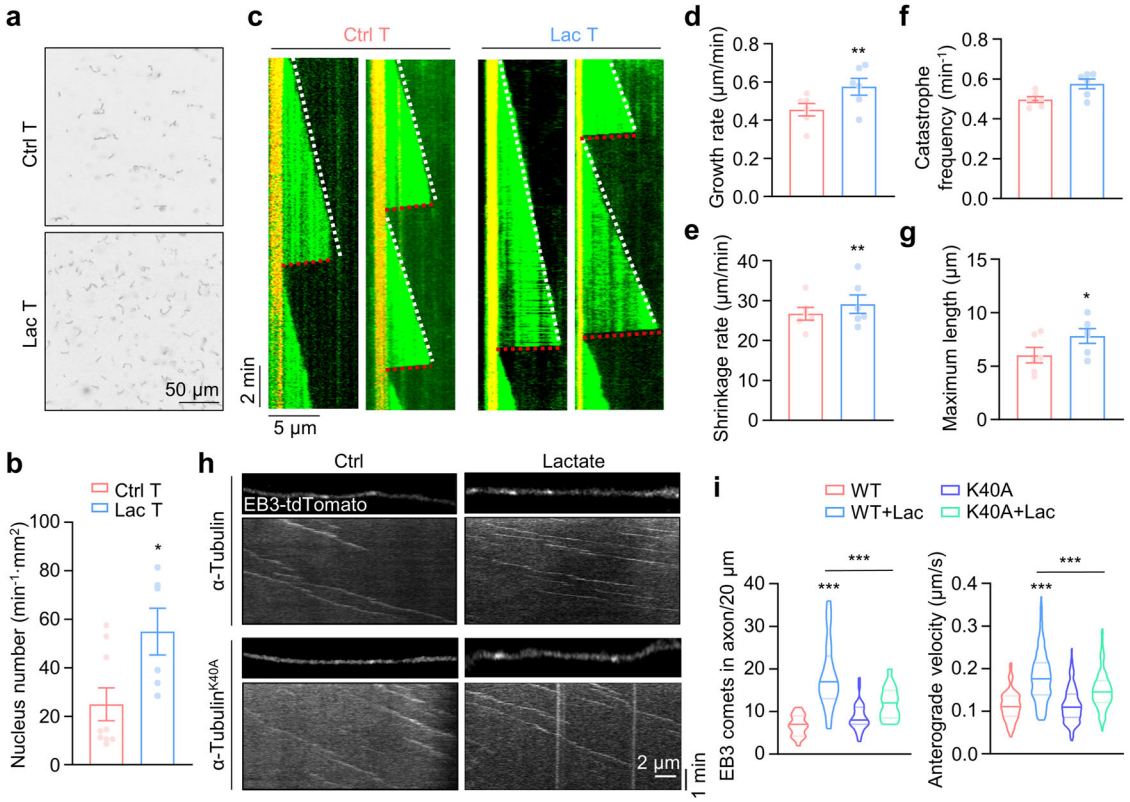

Fig. 5 | α-Tubulin lactylation promotes microtubule polymerization and dynamics. a Representative images of tubulin nucleation assay using 15 μM native or in vitro lactylated α-tubulin. Free tubulin comprising unlabeled and HiLyte-488-tubulin at a 9:1 ratio were incubated with 1 mM GTP and 5% glycerol at 37 °C for 30 min. **b** Quantitative analysis of data in (**a**). Ctrl T, n = 9; Lac T, n = 6. Two-sided unpaired student's *t*-test, p = 0.0210. **c** Representative Kymographs of dynamic microtubules from α-tubulin or lactylated-α-tubulin by time-lapse imaging with TIRF microscopy. Quantitative analysis of microtubule growth rate in (**d**), shrinkage rate in (**e**), catastrophe frequency in (**f**), and maximum length in (**g**). n = 6 experiments. Two-sided paired student's *t*-test, for growth rate, p = 0.0026; for shrinkage rate, p = 0.0042; for maximum length, p = 0.0295. **h** Representative images and kymographs of EB3-tdTomato in cultured hippocampus neurons at DIV3. The neurons were transfected with EB3-tdTomato together with α-tubulin or α-tubulin K40A mutant, were then cultured with or without 30 mM lactate. **i** Quantitative analysis of number of EB3 comets and anterograde velocity. EB3 comets: WT, n = 20; WT + Lac, n = 21; K40A, n = 31; and K40A + Lac, n = 17 neurons from 3 experiments. Anterograde velocity: WT, n = 112; WT + Lac, n = 301; K40A, n = 194; and K40A + Lac, n = 236 EB3 comets from 3 experiments. One-way ANOVA, for EB3 comets, WT + Lac vs WT, p < 0.0001; K40A + Lac vs WT + Lac, p < 0.0001. For anterograde velocity, WT + Lac vs WT, p < 0.0001; K40A + Lac vs WT + Lac, p < 0.0001. Data are shown as mean ± SEM. *p < 0.05, **p < 0.01, ***p < 0.001. Source data are provided as a Source Data file.

α-Tubulin lactylation enhances neurite outgrowth and branching

We further examined whether α-tubulin lactylation regulates microtubule dynamics in cultured neurons. Microtubule plus ends were labeled by EB3-tdTomato and time-lapse imaging was performed to determine the microtubule dynamics in hippocampal neurons at day in vitro (DIV) 3. Quantitative analysis revealed a significant increase in the number of EB3 comets in axons treated with lactate, and this increase was restored by expressing the α-tubulin^{K40A} mutant (Fig. 5h, i), suggesting that α-tubulin lactylation may increase the growing microtubule numbers probably through enhanced tubulin nucleation in neurons. Additionally, lactate treatment increased the velocity of EB3 comets in axons (Fig. 5h, i), indicating that α-tubulin lactylation may increase microtubule dynamics in cultured neurons.

To explore the functional roles of α-tubulin lactylation in neurite outgrowth, we investigated the neurite outgrowth in cultured hippocampal neurons. Control hippocampal neurons at DIV3 typically displayed a polarized morphology with one SMI-312-positive axon and several dendrites. However, the polarization percentage was reduced in lactate-treated neurons, which displayed multipolar morphologies (Fig. 6a, b). Furthermore, lactate treatment increased the number of neurite tips and branching (Fig. 6a, b). These alterations induced by lactate could be restored by the α-tubulin^{K40A} mutant (Fig. 6a, b). To exclude the potential toxicity of lactate on neurons, we treated primary cultured neurons with various concentrations of lactate and assessed cell viability using the CCK8 assay. As shown in supplementary Fig. 6, lactate treatment had little effect on neuronal viability. These results suggest that α-tubulin lactylation plays important roles in regulating neuronal development and nerite outgrowth.

To assess the potential impact of α-tubulin lactylation on axonal regrowth after injury, cortical neurons were plated on one-half part of the dish to separate extended axons from cell bodies. After 7 days of culture, axons extended into the other half of the dish. We severed axons without affecting cell bodies and measured axon extension to assess regrowth after injury. Our results revealed significantly increased regrowth in the lactate-treated neurons, and the α-tubulin^{K40A} mutant abolished the lactate-induced increment (Fig. 6c, d).

The conservation of lactylation catalytic activity among HDACs

Finally, we wanted to determine whether the lactylation activity is conserved among HDAC family proteins. We examined several microtubule-associated proteins (MAPs) previously identified as lactylated in mass spectrum analysis (Fig. 1b, supplementary Fig. 7a and supplementary Fig. 8a). When these proteins were transfected into HEK293T cells along with HDAC family proteins, we observed distinct patterns of lactylation. Specifically, HDAC3 increased lactylation of EB3 (Supplementary Fig. 7b, c). To further validate this, we

https://doi.org/10.1038/s41467-024-52729-0

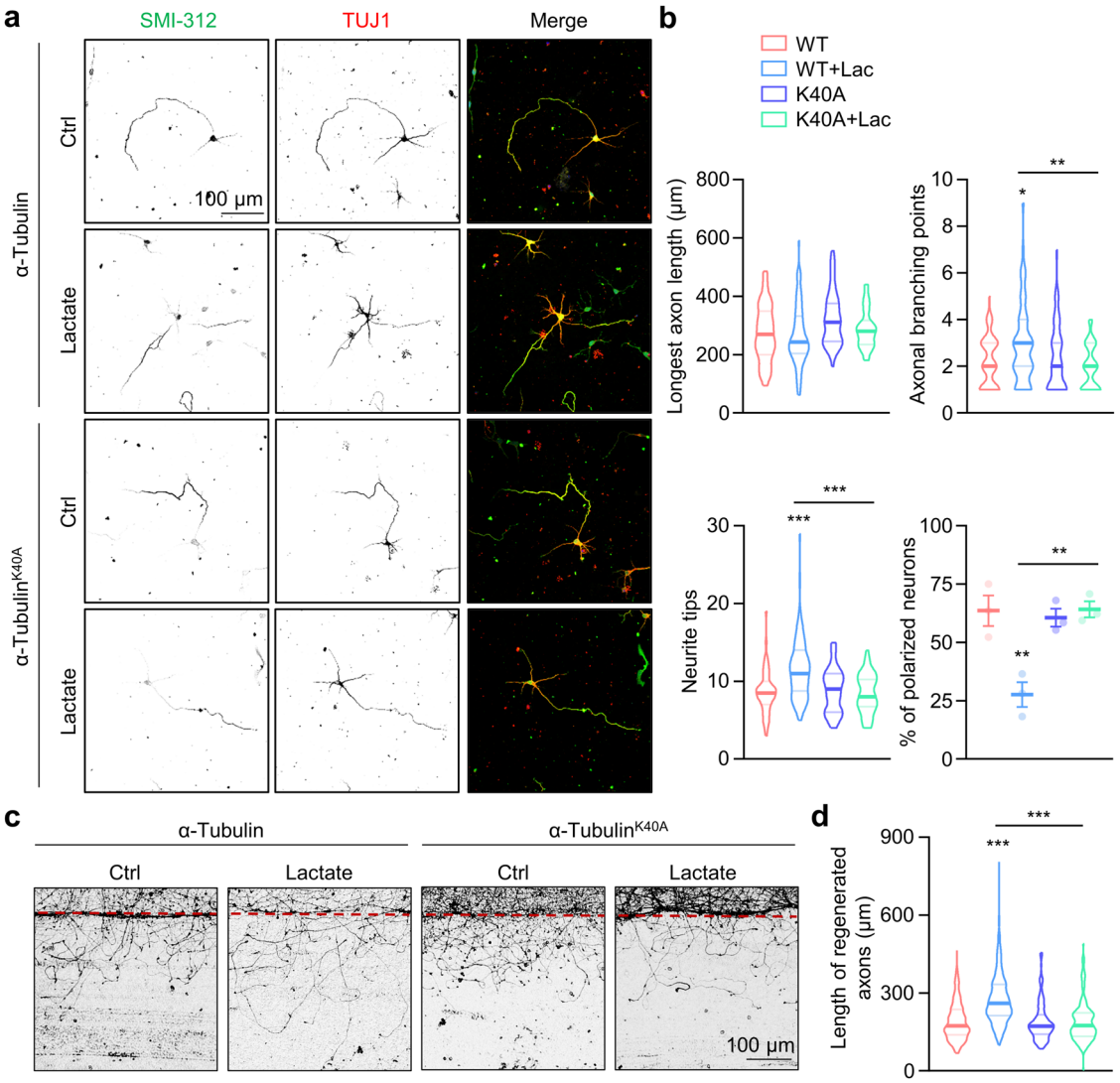

Fig. 6 | α-Tubulin lactylation promotes axon outgrowth and branching. **a** Representative images of hippocampal neurons at DIV3. The hippocampal neurons were transfected with α-tubulin or α-tubulin K40A mutant. The neurons were treated with 30 mM lactate for 72 h, and stained with anti-SMI-312 (green) and anti-Tuj-1 (red) antibodies. **b** Quantitative analysis of the longest axon length, number of axonal branching points, number of neurite tips, and percentage of polarized neurons in cultured neurons in (**a**). For WT, WT + Lac, K40A, and K40A + Lac, n = 66, 74, 54, and 62 neurons, respectively, from 3 experiments. One-way ANOVA, for axonal branching points, WT + Lac vs WT, p = 0.0265; K40A + Lac vs WT + Lac, p = 0.0024. For neurite tips, WT + Lac vs WT, p < 0.0001; K40A + Lac vs WT + Lac, p < 0.0001. For polarized neurons, WT + Lac vs WT, p = 0.0039; K40A + Lac vs WT + Lac, p = 0.0035. **c** Representative images of axon regeneration. The cortical neurons were infected with lentiviruses encoding α-tubulin or α-tubulin K40A mutant. The axons were severed after being treated with or without 30 mM lactate for 4 h at DIV7 and axon regeneration was assessed 1 day later. **d** Quantitative analysis of data in (**c**). For WT, WT + Lac, K40A, and K40A + Lac, n = 222, 221, 175, and 159 axons, respectively, from 3 experiments. One-way ANOVA, WT + Lac vs WT, p < 0.0001; K40A + Lac vs WT + Lac, p < 0.0001. Data are shown as mean ± SEM. *p < 0.05, **p < 0.01, ***p < 0.001. Source data are provided as a Source Data file.

generated HDAC3 KO cells and observed a significant decrease in EB3 lactylation levels (Supplementary Fig. 7d, e). The acetylation level of EB3 remained unchanged when HDAC3 or HDAC6 were overexpressed (Supplementary Fig. 7f, g). This suggests that the increase in EB3 lactylation by HDAC3 is not due to a decrease in acetylation. The deacetylase activity of HDAC3 is necessary for its lactyltransferase activity, evidenced by the abolishment of EB3 lactylation in cells treated with HDAC inhibitor TSA (Supplementary Fig. 7h, i), or in cells expressing a deacetylase-dead mutant HDAC3-C145S (Supplementary Fig. 7j, k). Moreover, HDAC3 KO resulted in decreased global protein lactylation (Supplementary Fig. 7l, m). Similarly, DCX lactylation was catalyzed by HDAC3 and HDAC6 (Supplementary Fig. 8). These findings support the conservation of lactylation activity within HDAC family proteins.

Discussion

In summary, our results support a model in which glycolysis regulates cytoskeleton functions by α-tubulin lactylation (Fig. 7). The intracellular glycolysis, which produces lactate, enhances α-tubulin lactylation catalyzed by HDAC6. This modification competes with α-tubulin acetylation to enhance microtubule dynamics. Furthermore, the MAPs are also catalyzed by HDAC family proteins, especially HDAC3 and HDAC6. Lactylation on MAPs might regulate their binding affinity to microtubules, thereby influencing cytoskeleton functions (Fig. 7). Our findings establish a link between cell metabolism to cytoskeleton functions.

Protein lactylation has been shown to be mediated by acetyltransferases and reversed by deacetylases[45,49]. Acetyltransferases such as p300 or TIP60 catalyze protein lactylation by using Lac-CoA as the

https://doi.org/10.1038/s41467-024-52729-0

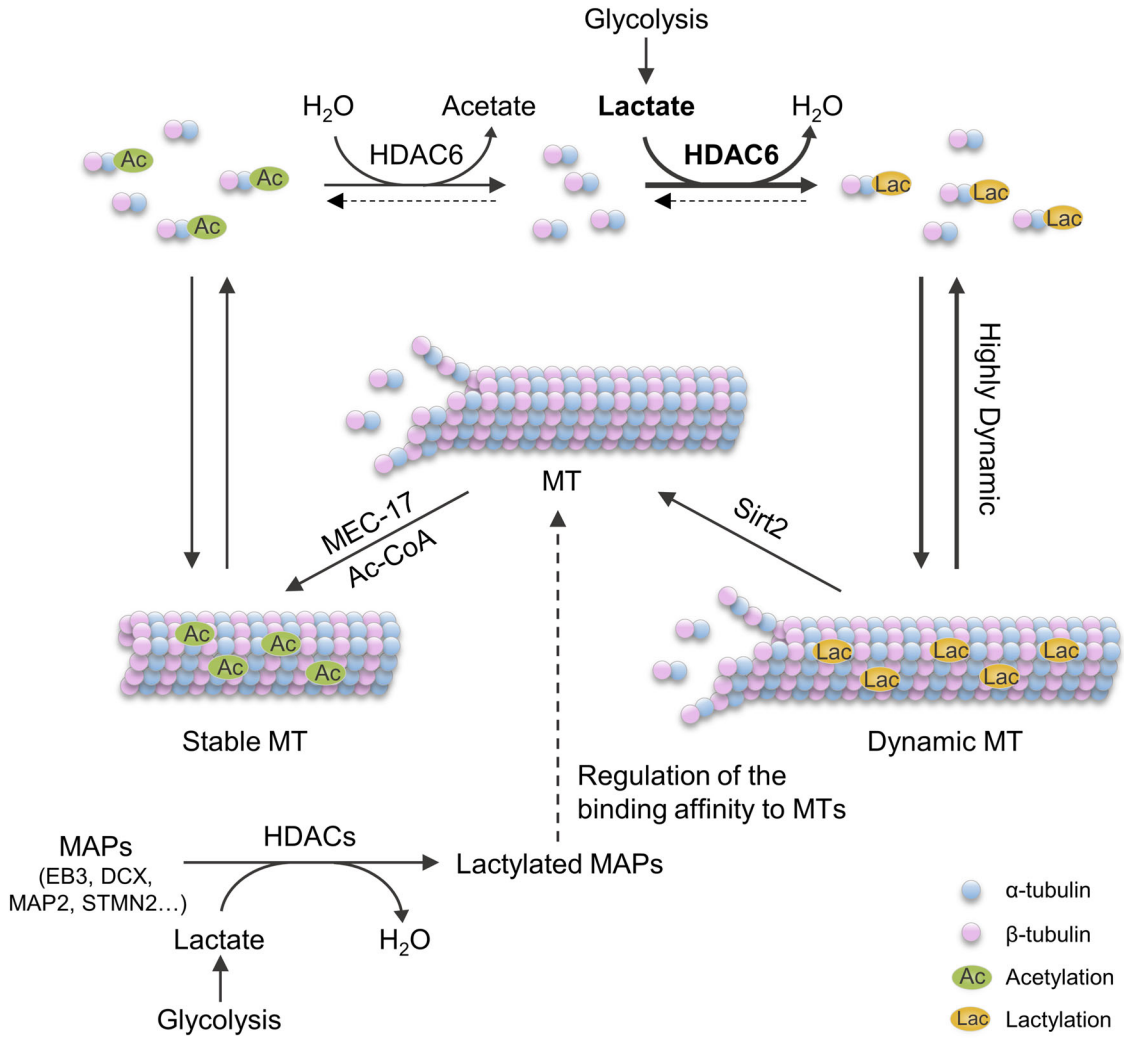

Fig. 7 | A proposed model for the regulation of α-tubulin lactylation. The glycolysis is crucial for energy generation in cells and results in the production of lactate. HDAC6 functions as a lactyltransferase to lactylate the α-tubulin K40 residue by using lactate, facilitating microtubule dynamics. HDAC3 catalyzes lactate to enhance lactylation of microtubule-associated proteins that may also affect cytoskeleton functions.

lactyl donor[27,32], while histone deacetylases and Sirtuins have been implicated in the removal of protein lactylation[33,34]. In this study, we identified the function of HDAC6 as a lactyltransferase for α-tubulin lactylation, which is supported by several pieces of evidence: First, HDAC6 overexpression led to increased α-tubulin lactylation (Fig. 2a), and HDAC6 deficiency caused a significant reduction in α-tubulin lactylation (Fig. 2c). Second, in vitro experiments revealed that HDAC6-catalyzed α-tubulin lactylation was a reversible reaction, indicating that high concentration of lactate drives the reaction from delactylation to lactylation (Fig. 3a). Third, the second catalytic domain of HDAC6 is critical for the lactyltransferase activity, and the residues involved in deacetylase activity are critical for catalyzing α-tubulin lactylation (Fig. 3l, m). Finally, we tested several MAPs identified in the mass spectrometry results and found that HDAC3 also serves as lactyltransferase for MAPs (Supplementary Fig. 7 and supplementary Fig. 8). Notably, it is possible that other HDAC family proteins may also possess the lactyltransferase activity, especially considering that the proteins examined in this study were exclusively cytosolic. This suggests a potential conserved function among HDAC proteins in acting as lactyltransferases to control protein lactylation.

Protein posttranslational modifications are dynamically regulated by the metabolic state in cells. The metabolites often function as modification donors to covalently conjugate to protein substrates. For example, acetyl-coenzyme A (Ac-CoA) and S-adenosylmethionine (SAM) can be catalyzed by acetyltransferases for lysine acetylation and by methyltransferases for lysine methylation, respectively[50,51]. The Lac-CoA is believed to be the lactyl donor catalyzed by acetyltransferases to increase protein lactylation[45]. Moreover, lactylglutathione (LGSH), an intermediate in the glyoxalase pathway, can serve as a lactyl donor by reacting nonenzymatically to promote lysine lactylation on glycolytic enzymes[37]. However, the Lac-CoA concentration is about 10 nM compared to 10 μM Ac-CoA in the cytosol[31]. Therefore, the acetyltransferases mainly regulate protein acetylation instead of lactylation, due to much higher Ac-CoA concentration in cells. Indeed, the deficiency of MEC-17 resulted in the elimination of α-tubulin acetylation, although it had a relatively minor impact on α-tubulin lactylation (Supplementary Fig. 1i, j), suggesting acetyltransferases and Lac-CoA may not play a primary role in regulating protein lactylation.

It is believed that lactate is converted into Lac-CoA to promote protein lactylation[27,45]. However, our study discovered that lactate could directly conjugated onto lysine residues catalyzed by HDAC6. In vitro experiments showed that high lactate concentration triggered HDAC6 to lactylate α-tubulin (Fig. 3a). This notion was further supported by the observation that lactate treatment increased α-tubulin lactylation in WT cells and MEC-17-deficient cells (Supplementary Fig. 1i),

but not in HDAC6-deficient cells (Supplementary Fig. 3o). Moreover, the intracellular lactate concentration can range from about 2 mM to 30 mM[40–42], much higher than Lac-CoA, and this concentration is enough to trigger HDAC6-catalyzed α-tubulin lactylation reaction (Fig. 3a). Importantly, HDAC6 plays a major role in regulating α-tubulin lactylation because HDAC6 deficiency led to a large reduction in α-tubulin lactylation (Fig. 2c, i). Together, these results demonstrate that lactate may be the major lactyl-group donor in regulating protein lactylation, catalyzed by HDAC proteins.

Dynamic instability is the key feature of microtubules that modulates microtubule properties and functions. The combinations of tubulin posttranslational modifications and tubulin isotypes could control microtubule dynamics and functions[1]. In this study, we discovered lactylation on K40 of α-tubulin, the same residue modified by acetylation (Fig. 1f). Interestingly, acetylated α-tubulin is enriched in the stable microtubules with longer lifetime, while lactylated α-tubulin is distributed in soluble tubulin dimers (Fig. 4a). Moreover, lactylated α-tubulin promotes tubulin nucleation and increases both the growth and shrinkage rates of microtubules (Fig. 5c–e). These observations demonstrate that lactylation modulate tubulin properties but in the opposite way to acetylation, making K40 residue on α-tubulin a molecular switch to alter microtubule dynamic instability. Additionally, our investigations into the functional roles of α-tubulin lactylation in cultured neurons revealed that lactylation enhances neurite outgrowth and branching, as well as axonal regeneration after injury (Fig. 6). However, the physiological relevance of α-tubulin lactylation in vivo remains unknown. During development, changes in glycolysis in neurons or glial cells may alter α-tubulin lactylation levels in neurons. Given that α-tubulin lactylation increases microtubule dynamics, alterations in α-tubulin lactylation may regulate neuronal morphogenesis, including dendritic morphology, axonal projection, or synapse formation. Furthermore, mitochondria dysfunction and lactate accumulation, frequently observed in neurodegenerative diseases, may lead to elevated α-tubulin lactylation. Increased α-tubulin lactylation could reduce microtubule stability in axons, impair axonal transport, and eventually result in neurodegeneration. However, the physiological and pathological functions of α-tubulin lactylation in vivo require further study.

α-Tubulin acetylation is a well-studied modification in the microtubule lumen and labels stable microtubules. Stable microtubules marked by acetylation probably result from the catalytic preference of the "writer" MEC-17 for microtubules and the "eraser" HDAC6's preference for tubulin dimers[16,17]. In contrast, the distribution of lactylated α-tubulin in tubulin dimers may also arise from the distinct substrate preference of the "writer" and "eraser". The primary "writer" HDAC6 preferred tubulin dimers over microtubules (Fig. 3f), whereas the "eraser" Sirt2 catalyzed α-tubulin delactylation in microtubules (Supplementary Fig. 4g) resulting in enriched α-tubulin lactylation in soluble tubulin dimers. Previous studies have demonstrated that α-tubulin acetylation reduces the lateral interactions between protofilaments and protects microtubules from repeated mechanical stress[11,12]. However, the mechanism by which α-tubulin lactylation regulates microtubule dynamics needs to be further studied.

Methods

Materials

Pan anti-Kla (PTM-bio, Cat# PTM-1401), anti-acetylated tubulin (Sigma, Cat# T7451), anti-HA tag (Abmart, Cat# M20003), anti-HA tag (Sigma, Cat# H6908), anti-Flag tag (Abmart, Cat# M20008), anti-Flag tag (Sigma, Cat# F7425), anti-GFP (Thermo Fisher Scientific, Cat# A-11122), anti-α-tubulin (Santa Cruz, Cat# sc-32293), anti-α-tubulin (Proteintech, Cat# 11224-1-AP), anti-HDAC6 (Proteintech, Cat# 12834-1-AP), anti-β3-Tubulin (Cell Signaling technology, Cat# 5568), anti-β3-Tubulin (Merck/Millipore, Cat# MAB1637), Purified anti-Neurofilament Marker (SMI-312, BioLegend, Cat# 837904), anti-Sirt2 (PTM-bio, Cat# PTM-6318), anti-HDAC3 (PTM-bio, Cat# PTM-5183), Phalloidin-iFluor 633 Reagent (Abcam, Cat# ab176758), Sodium L-lactate (Sigma, Cat# 71718), Lactyl coenzyme A (Chemsoon, Cat# FM120), GSK2837808A (GSKA, TargetMol, Cat# T15435), D-(+)-Glucose (Sigma, G7021), 2-Deoxy-D-glucose (APExBIO, Cat# B1027), Rotenone (TargetMol, Cat# T2970), Nocodazole (APExBIO, Cat# A8487), Paclitaxel (Taxol) (APExBIO, Cat# A4393), NAD+ (Santa Cruz, Cat# sc-208084B), Trichostatin A (TSA) (APExBIO, Cat# A8183), Tubastatin A (TST) (Selleck, Cat# S8049), Biotin-tubulin (Cytoskeleton, Cat# T333P-A), Rhodamine-tubulin (Cytoskeleton, Cat# TL590M-A), HiLyte-488-tubulin (Cytoskeleton, Cat# TL488M-A), GMPCPP (Jena Biosciences, Cat# NU-405S).

Plasmids

Flag-p300, Flag-HDAC1, Flag-HDAC2, Flag-HDAC3, Flag-HDAC5, Flag-HDAC7, Flag-HDAC9 were acquired from BIO-RESEARCH INNOVATION CENTER SUZHOU. Flag-Sirtuins were gifts from Dr. Gaofeng Fan in Shanghaitech University. Plasmid HA-α-tubulin-1A/1C/3B/4 A/8, GFP-MEC-17, GST-MEC-17, and EB3-tdTomato were gifts from Dr. Lan Bao in CAS Center for Excellence in Molecular Cell Science, Chinese Academy of Sciences.

Cell culture and transfection

HEK293T cells were cultured in Dulbecco's Modified Eagle Medium (DMEM, Gibco) supplemented with 10% fetal bovine serum (Gibco) and antibiotics (ABCONE). Transient transfection was performed using PEI 40000 (Yeasen), and subsequent assays were conducted 36 h after transfection. For hypoxia treatment, HEK293T cells were transferred to a hypoxia incubator with a gas mixture containing 5% CO2 and 1% O2 balanced with nitrogen, harvested after 24 h.

Primary neurons were cultured as previously described[52]. The mouse hippocampus and cortex were dissected at postnatal day (P0) in Hank's balanced salt solution (HBSS, CellGro) and digested with 0.25% trypsin (Gibco) for 15 min at 37 °C. After digestion, the tissues were washed three times in DMEM and dissociated by repeated passaging through a 1 ml pipette. The neurons were then plated on poly-D-lysine (Sigma) coated dishes with DMEM containing 10% fetal bovine serum. After 2 h, the medium was replaced by Neurobasal medium (Gibco) containing 2% B-27 supplement (Gibco) and 2 mM GlutaMAX-I (Gibco). Half media changes were performed every 3 days. For neuron growth experiment, lentivirus was added to hippocampal neurons 2 h after plating and removed after 12 h treatment. For EB3 time-lapse imaging, the indicated plasmids were transfected into hippocampal neurons by Lipofectamine LTX (Thermo) 12 h after plating and removed after 12 h treatment. The neurons were used for immunostaining or time-lapse imaging at DIV3. For neuronal cytotoxicity assay, primary cultured neurons were treated with various concentrations of lactate for 72 h and cell viability was determined by the CCK8 assay kit (Beyotime).

Peptide Immunoprecipitation

Primary cortical neurons obtained from C57/BL6J mice at P0 were lysed directly with 8 M urea. The supernatant was diluted with 50 mM NH_4HCO_3 buffer to decrease the urea concentration to 1 M. Subsequently, the proteins were digested into peptides by trypsin overnight at 37 °C. The peptides were incubated with protein A/G agarose beads (Abmart) immobilized with Pan lactylated-lysine antibody for 4 h at 4 °C. Peptides were eluted from the beads with 0.1% TFA, followed by desalting on a Sep-pak C18 cartridges column and subsequent vacuum lyophilization. The vacuum-dried samples were resuspended in 0.1% FA for liquid chromatography (LC)-MS/ MS analysis.

HPLC/MS/MS analysis

The peptide samples were loaded and separated by a C18 analytical column (75 μm ID × 15 cm, 1.9 μm, self-pack). The separation and analysis of peptides were carried out using an Easy-nLC 1200 system

coupled to a Q-Exactive HF Hybrid Quadrupole-Orbirap Mass spectrometer system (Thermo Fisher Scientific). A 60-min gradient was established using mobile phase A (0.1% formic acid) and mobile phase B (0.1% formic acid in 98% ACN), consisting of 51 min of 2–28% B, 1 min of 28–38% B, 1 min of 38–90% B, and 7 min of 90% B, at a constant flow rate of 300 nL/min at 45 °C. Electrospray ionization at 2.2 kV was employed for peptide ionization. Full scan MS spectra (from m/z 375 to 1500) were acquired in the Orbitrap at a high resolution of 60,000 with an automatic gain control (AGC) of 5e5 and a maximum fill time of 50 ms. The twenty most intense ions were sequentially isolated and fragmented in the HCD collision cell with normalized collision energy of 25%. Fragmentation spectra were acquired in the Orbitrap analyzer with a resolution of 15,000. Ions selected for MS/MS were dynamically excluded for a duration of 10 s.

Proteomic analysis was performed using the Gene Ontology tool from the DAVID Bioinformatics (https://david.ncifcrf.gov). Enriched GO molecular functions were identified and listed according to their enrichment p-values ($p < 0.05$). The mass spectrometry proteomics data have been deposited to the ProteomeXchange Consortium (https://proteomecentral.proteomexchange.org) via the iProX partner repository with the dataset identifier PXD055797.

Immunoblotting and immunoprecipitation

Immunoblotting was performed as described previously[43,52]. Cells were lysed in common RIPA buffer (50 mM Tris-HCl pH 7.5, 150 mM NaCl, 1% Triton X-100, 10% glycerol and protease inhibitor Cocktail (APExBIO)) and the brain tissues were lysed in RIPA Lysis Buffer (Beyotime) (50 mM Tris pH 7.4, 150 mM NaCl, 1% Triton X-100, 1% sodium deoxycholate, 0.1% SDS). Protein samples were separated by SDS-PAGE, transferred to the nitrocellulose membrane (Cytiva), blocked by 5% skim milk for 30 min at room temperature, probed with specific antibodies and then visualized with Omni-ECL™ Femto Light Chemiluminescence Kit (Epizyme). Images were captured with Tanon 5200 and analyzed using ImageJ software.

For dot blotting, indicated peptides were spotted onto the nitrocellulose membrane. The membrane was blocked with 5% skim milk after air-drying and then incubated indicated antibodies.

For the co-immunoprecipitation experiment, cells were lysed in RIPA buffer. Following centrifugation, the supernatant was incubated with anti-HA IP resin (Genescript) at 4 °C for 2 h and directly eluted with 1× loading buffer (2.5 mM Tris-HCl pH 6.8, 2% SDS, 0.1% Bromophenol blue, 10% glycerol, 8% 2-Hydroxy-1-ethanethiol in ddH_2O). The immunoprecipitated samples were analyzed by immunoblotting.

Protein expression and purification

GST-tagged proteins were purified as previously described[53]. The mouse MEC-17 containing residues 1–193 or the full-length human Sirt2 was subcloned into pGEX-2T expression vector and expressed in *E. coli* BL21 at 37 °C for 4 h. Subsequently, induction was carried out with 0.1 mM IPTG (ABCONE) at 16 °C for 16 h. Cells were collected by centrifugation at 6000 × *g* for 10 min, and cell pellets were resuspended with lysis buffer (PBS pH 7.4, 1 mM DTT (ABCONE), Cocktail) followed by sonication at 4 °C. Cell fragments were removed by centrifugation at 12,000 × *g* for 20 min at 4 °C. The lysates were then incubated with GST-tag purification resin (Beyotime) for 4 h and rinsed with PBS (pH 7.4). Proteins were collected in the elution buffer (50 mM Tris-HCl pH 8.0, 150 mM NaCl, 20 mM reduced L-glutathione (Sigma)), which was subsequently replaced by PBS. The proteins were concentrated, quantitatively analyzed, frozen by liquid nitrogen, and stored at −80 °C.

For Flag-HDAC6, the purification was performed as previously described[54]. The full-length human HDAC6 was expressed in 293S cells. The cell pellet was re-suspended in 100 ml buffer containing PBS pH 7.4, 300 mM NaCl, 10 mM $MgCl_2$, 10% glycerol, and 1 ml protease inhibitor cocktail (EDTA-Free, 100x in DMSO; ApexBio), followed by sonication for cell lysis. The cell lysate was then centrifuged at 24,300 x *g* for 40 min at 4 °C. The supernatant obtained was incubated with Flag beads (Smart-Lifesciences) for 2 h at 4 °C. The beads were then washed 4 times with 50 bed volumes of wash buffer (PBS pH 7.4, 463 mM NaCl, 1 mM DTT) and eluted with a buffer containing 50 mM HEPES pH 7.5 and 150 mM NaCl. The protein was further purified by chromatography using a HiLoad 16/600 Superdex 200 pg column (Cytivia) (AKTA). The collected peak fraction was concentrated, quantitatively analyzed, frozen by liquid nitrogen, and stored at −80 °C.

Tubulin purification and lactylated tubulin preparation

Tubulin purification from the brains of adult C57/BL6J mice involved two cycles of polymerization/depolymerization as previously described[55]. The tubulin was firstly deacetylated by purified GST-Sirt2 with 5 mM NAD+ in the depolymerization buffer (DB, 50 mM MES pH 6.6, 1 mM $CaCl_2$) at 4 °C for 30 min for depolymerization, and then at 37 °C for 1 h for deacetylation, followed by another 4 °C for 30 min for depolymerization for the next cycle. The low acetylated tubulin obtained was polymerized in HMPB (1 M PIPES/KOH pH 6.9, 10 mM $MgCl_2$, 20 mM EGTA, 50% glycerol, 1.5 mM ATP (Sigma), 0.5 mM GTP (Sigma)) at 37 °C for 30 min to remove Sirt2 by centrifugation. Subsequently, GST-MEC-17 (1–193) protein and 10 μM Lac-CoA were added to the depolymerization buffer for α-tubulin lactylation at 37 °C for 1 h and removed through two cycles. The lactylated tubulin was dissolved in cold BRB80 buffer (80 mM PIPES-KOH pH 6.8, 1 mM EGTA, 1 mM $MgCl_2$) and frozen by liquid nitrogen and stored at −80 °C.

In vitro α-tubulin lactylation and delactylation assays

The MEC-17 lactyltransferase assays were performed in a buffer that was used for histone acetyltransferase assays, containing 50 mM Tris-HCl pH 8.0, 10% glycerol, 0.1 mM EDTA, 1 mM DTT. The reaction mixture included 10 μM Lac-CoA, purified GST-MEC-17, 1 mM GTP, and tubulins from the brain. The reaction lasted for 1 h or the indicated time at 37 °C. The HDAC6 lactylation assays were performed in BRB80 buffer containing 80 mM PIPES-KOH pH 7.4, 1 mM $MgCl_2$, 1 mM EGTA. The reaction mixture included purified Flag-HDAC6, tubulins from brain and lactate with indicated concentrations. The reaction lasted for 1 h or the indicated time at 37 °C. The Sirt2 delactylation assays were performed in BRB80 buffer (pH 6.8). The reaction mixture included purified GST-Sirt2 and tubulins from brain or 1 mM NAD+. The reaction lasted for 1 h or the indicated time at 37 °C.

All the reactions were stopped by adding 2× or 4× loading buffer, followed by heating for 7 min at 98 °C and subjected to immunoblotting.

Preparation of tubulin polymers

To obtain Taxol-stabilized microtubules (MTs), tubulins at a concentration of 6 mg/ml was polymerized for 30 min at 37 °C in BRB80 buffer (pH 6.8) supplemented with 4.8% DMSO, 1 mM GTP and 20 μM Taxol. Following polymerization, the polymers were pelleted at 30,000 × *g* for 40 min at 37 °C, and the resulting pellet was suspended in warm BRB80 (pH 6.8) with 20 μM Taxol to achieve the required concentration and stored at room temperature.

Cell line gene editing

CRISPR-Cas9 gene-modified cells were generated as previously described[53]. Briefly, the guidance RNAs were inserted into BbsI site of PX330-GFP construct and verified by sequencing. The constructs were transfected into HEK293T cells by PEI 40,000. After 48 h, the GFP-positive cells were sorted by FACS and seeded into the 96-well plate, with each well containing a single cell. The cloned cells derived from an individual cell were verified by genomic DNA sequencing and Immunoblotting. The sequence of sgRNAs is as follows, MEC-17 sgRNA 5′-CCGACCCGGAACCACAACGC-3′ and HDAC6 sgRNA 5′-ACAACCAGGCAGCGAAGAAGT-3′, Sirt2 sgRNA 5′-CTACTTCATGCGCCTGCTGA-3′ and HDAC3 sgRNA 5′-ACGGTGTCCTTCCACAAATA-3′.

Generation of the antibody against α-tubulin K40 lactylation

The antibody against α-tubulin K40 lactylation was custom-designed and generated by HUA BIO, Zhejiang, China. The control peptide (DGQMPSDKTIGGGDDC), the acetylated peptide [DGQMPSDK(Ac)TIGGGDDC], and the lactylated peptide [DGQMPSDK(Lac)TIGGGDDC] were synthesized. The lactylated peptide served as the immunogen for raising the specific antibody in rabbits. Initial purification of α-tubulin K40 lactylation-specific antibody involved negative screening using serial columns with control and acetylated peptides. Subsequently, specific affinity purification was carried out using lactylated peptides.

Measurement of the soluble and polymerized tubulin fractions

HEK293T cells were lysed with pre-warmed BRB80 (pH 6.8) supplemented with 0.5% Triton X-100 for 5 min, followed by centrifugation at 17,400 × *g* for 10 min at room temperature. The supernatant, denatured with 4x loading buffer, used as soluble tubulin fraction (S). The pellet, containing microtubules, was reconstituted with cold BRB80 buffer and kept on ice for 15 min to include microtubule depolymerization. After centrifugation at 5000 x *g* for 10 min, the supernatant was denatured and used as the polymerized microtubule fraction (P).

HDAC6 kinetic assay

The kinetic parameters of HDAC6 were determined by an in vitro lactylation assay. Lactylated α-tubulin was quantified using a standard curve generated from a dot blot assay by using the synthesized peptide (TUBA1A: DGQMPSDK(Lac)TIGGGDDC) containing K40 lactylation. The peptide was diluted with ddH_2O to the indicated dilutions and then was blotted onto nitrocellulose membranes, followed by air drying at room temperature to immunoblots. The HDAC6 lactylation assays were performed in BRB80 (pH 7.4). 4 μM purified HDAC6 as the enzyme, 2 μM purified tubulin heterodimers as the substrate, and various concentrations of lactate ranging from 5 mM to 160 mM. The reaction time points were set at 10, 20, and 30 min at 37 °C to determine the K_m and K_{cat} of HDAC6 for lactate. K_m and K_{cat} were deduced using the Michaelis-Menten equation using Prism 8.0.2 software (GraphPad).

Immunostaining

Immunostaining was performed as described previously[52]. The cultured neurons were fixed with 4% paraformaldehyde (PFA) for 20 min at room temperature, blocked by the immunostaining buffer (1% BSA, 0.5% Triton X-100 in PBS) for 15 min at room temperature, and subsequently incubated with primary antibodies diluted in the immunostaining buffer overnight at 4 °C. Following washing steps, samples were incubated with the Alexa-Fluor-conjugated secondary antibodies for 45 min at 37 °C, followed by staining with Hoechst (Meilune) for 10 min at room temperature.

For growth cone staining, cultured neurons were fixed with 2% glutaraldehyde in PHEM buffer (60 mM PIPES pH 6.9, 25 mM HEPES, 10 mM EGTA, 2 mM $MgCl_2$ and 1 mg/ml sodium borohyride) for 15 min. To facilitate permeabilized labeling, 1% Triton X-100 was added into the fixative to remove the membranes and soluble substances, allowing the retention of cytoskeletal components and their associated proteins. Subsequently, the cultured neurons were immunostained with primary antibodies for 48 h at 4 °C. Following washing steps, phalloidin-staining was performed by incubating with phalloidin-633 (Abcam) at 37 °C for 60 min.

Fluorescent images were acquired using the Zeiss 980 Upright microscope and analyzed using ImageJ software.

Microtubule nucleation assay

The microtubule nucleation assay was performed as descripted previously[26]. Briefly, a mixture of 15 μM free tubulins (comprising unlabeled and HiLyte-488-tubulin at a 9:1 ratio) were incubated at 37 °C for 30 min in BRB80 buffer (pH 6.8) supplemented with 1 mM GTP and 5% glycerol. Microtubules were fixed with 0.5% glutaraldehyde in BRB80 buffer (pH 6.8) for 15 min, and then centrifuged through a glycerol cushion onto a coverslip. The microtubules were imaged using Zeiss 980 Upright microscope equipped with a 63× oil immersion objective. The microtubules were counted using imageJ software.

In vitro microtubule reconstitution assay

To generate rhodamine-labeled GMPCPP-stabilized microtubule seeds through two cycles of polymerization, a mixture of unlabeled mouse brain tubulin dimers (1 mg/ml), biotin-tubulin (Cytoskeleton) at a concentration of 0.1 mg/ml and rhodamine-tubulin (Cytoskeleton) at a concentration of 0.1 mg/ml was incubated with 1 mM GMPCPP (Jena Biosciences) at 37 °C for 30 min. The mixture was then subjected to centrifugation at 126,000 × *g* for 5 min at 37 °C to remove unpolymerized tubulin. The microtubule pellet was resuspended in cold BRB80 (pH 6.8), followed by depolymerization at 4 °C for 20 min and a second round of polymerization with 1 mM GMPCPP for 30 min at 37 °C. Finally, microtubule seeds were obtained after centrifugation at 126,000 x *g* for 5 min at 37 °C, resuspended using 37 °C pre-warmed BRB80 (pH 6.8), frozen by liquid nitrogen and stored at −80 °C.

For the assembly of sample chamber, a cleaned and silanized glass coverslip was attached onto microscopic slides by double-sided tape to create a reaction space. A mixture of control tubulin or lactylated tubulin and HiLyte-488 labeled tubulin (at a 19:1 ratio) was prepared in BRB80 (pH 6.8) reaction buffer containing 5 mM Dithiothreitol (DTT), 0.1% methylcellulose, 75 mM KCl, 0.25 mg/mL bovine serum albumin (BSA), 25 mM glucose, 25 μg/ml catalase, 50 μg/ml glucose oxidase and 1 mM GTP. For the microtubule growth assay, microtubule seeds were flowed through the channel for 8 min at 37 °C before adding the reaction buffer. The sealed chamber was placed into Nikon Ti2-E TIRF Microscope with a pre-warmed 37 °C temperature-controlled workstation. Microtubule growth images were acquired with a 60× oil immersion 1.49 NA TIRF objective and Prime 95B Scientific CMOS (sCMOS) camera every 3 s for 15 min. Kymographs were generated and further analyzed using ImageJ software.

Time-lapse imaging

To detect the movement of EB3 in axons, hippocampal neurons were transfected with EB3-tdTomato and either pCDH-TUBA1A-ires-copGFP or pCDH-TUBA1A^{K40A}-ires-copGFP after planting on glass-bottom dishes for 12 h. And then the neurons were treated with 30 mM lactate for 12 h before time-lapse imaging. At DIV3, the dishes were placed on a temperature-controlled workstation (37 °C, 5% CO_2) with an inverted microscope and positive neurons were captured using Zeiss LSM 980 Airyscan under 10x objective for 5 min at 2 s intervals. Kymographs were generated and further analyzed using ImageJ software.

Primary neurons axotomy and axon regeneration

Primary cortical neurons from C57/BL6J mice at P0 were densely plated onto 15 mm glass bottom cell culture dish (NEST), with half of them tightly precoated with the sterile parafilm (Bemis). After 2 h, the DMEM containing 10% fetal bovine serum medium was replaced by Neurobasal medium containing 2% B-27 supplement and 2 mM GlutaMAX-I. The parafilm was removed after 12 h of neuron plating to mechanically clear cells from the designated culture area. Lentivirus was introduced to the neurons and removed after 12 h of treatment. The neurons were scratched using a 10 μl pipette tip at a position 600–800 μm distal from the soma after being treated with or without 30 mM lactate for 4 h at DIV7. The axons were allowed to regenerate for 24 h from pre-existing neurites before fixation by 4% PFA for regeneration quantification. The images were captured by Olympus CKX53 Microscope and analyzed using ImageJ software.

Animals

The MEC-17 KO mice were gifts from Dr. Lan Bao in CAS Center for Excellence in Molecular Cell Science, Chinese Academy of Sciences[22].

All animals used for immunoblotting were 2 months old and male. All animals used for tubulin purification were 2–6 months old and included both male and female. Mice were genotyped using primers (MEC-17-WT-forward: 5′-GGCTGCCAGGAATGACTTACACG-3′; MEC-17-WT-reverse: 5′-CAGGGAATAATGACAGTAAGACTCACG-3′; MEC-17-KO-forward: 5′-GCAGCCTCTGTTCCACATACACTTCA-3′; MEC-17-KO-reverse: 5′-TAGACTGTTTCCTGGGTTCTACTGCC-3′). The HDAC6 KO mice (#027068) were purchased from the GemPharmatech and genotyped using primers (HDAC6-WT-forward: 5′-GATGGCAGATACTTGCCAGAATG-3′; HDAC6-WT-reverse: 5′-GTACTGGGTTGTCTCCATCAGATC-3′; HDAC6-KO-forward: 5′-GGCTGCCAGGAATGACTTACACG-3′; HDAC6-KO-reverse: 5′-CAGGGAATAATGACAGTAAGACTCACG-3′).

All animal experiments including mouse housing and breeding were executed in compliance with the ethical guidelines of the Institutional Animal Care (IACUC) and Use Committee of ShanghaiTech University. All mice were housed under a 12-h light-dark cycle in the institutional animal care facility.

Statistics and reproducibility

Animal or replicate numbers for each experiment and results of the statistical analyses are mentioned in the Figure legends. All data were collected from at least 3 independent experiments and presented as the mean ± SEM. Statistical analysis was performed using Prism 8.0.2 software (GraphPad). Comparisons between two groups of immunoblots were evaluated by the student's *t*-test. Comparisons among multiple groups were performed with one-way ANOVA or two-way ANOVA. All tests were two-sided. The $p < 0.05$ was considered significant (*$p < 0.05$; **$p < 0.01$; ***$p < 0.001$).

Reporting summary

Further information on research design is available in the Nature Portfolio Reporting Summary linked to this article.

Data availability

The proteomic data generated in this study have been deposited in the ProteomeXchange database with dataset identifier number of PXD055797. All data associated with this study are available in the main text or the Supplementary Materials. All requests for reagents should be made to the corresponding authors upon reasonable request. They will be made available through appropriate administrative channels (MTA). Source data are provided with this paper.

References

1. Janke, C. & Magiera, M. M. The tubulin code and its role in controlling microtubule properties and functions. *Nat. Rev. Mol. Cell Biol.* **21**, 307–326 (2020).
2. Roll-Mecak, A. The tubulin code in microtubule dynamics and information encoding. *Dev. Cell* **54**, 7–20 (2020).
3. Tahirovic, S. & Bradke, F. Neuronal polarity. *Cold Spring Harb. Perspect. Biol.* **1**, a001644 (2009).
4. Conde, C. & Caceres, A. Microtubule assembly, organization and dynamics in axons and dendrites. *Nat. Rev. Neurosci.* **10**, 319–332 (2009).
5. Magiera, M. M., Singh, P., Gadadhar, S. & Janke, C. Tubulin posttranslational modifications and emerging links to human disease. *Cell* **173**, 1323–1327 (2018).
6. Wloga, D., Joachimiak, E., Louka, P. & Gaertig, J. Posttranslational modifications of tubulin and cilia. *Cold Spring Harb. Perspect. Biol.* **9**, a028159 https://doi.org/10.1101/cshperspect.a028159 (2017).
7. Piperno, G. & Fuller, M. T. Monoclonal antibodies specific for an acetylated form of alpha-tubulin recognize the antigen in cilia and flagella from a variety of organisms. *J. Cell Biol.* **101**, 2085–2094 (1985).
8. Schulze, E., Asai, D. J., Bulinski, J. C. & Kirschner, M. Posttranslational modification and microtubule stability. *J. Cell Biol.* **105**, 2167–2177 (1987).
9. Piperno, G., LeDizet, M. & Chang, X. J. Microtubules containing acetylated alpha-tubulin in mammalian cells in culture. *J. Cell Biol.* **104**, 289–302 (1987).
10. Takemura, R. et al. Increased microtubule stability and alpha-tubulin acetylation in cells transfected with microtubule-associated proteins MAP1B, MAP2, or tau. *J. Cell Sci.* **103**, 953–964 (1992).
11. Portran, D., Schaedel, L., Xu, Z., Thery, M. & Nachury, M. V. Tubulin acetylation protects long-lived microtubules against mechanical ageing. *Nat. Cell Biol.* **19**, 391–398 (2017).
12. Eshun-Wilson, L. et al. Effects of alpha-tubulin acetylation on microtubule structure and stability. *Proc. Natl. Acad. Sci. USA* **116**, 10366–10371 (2019).
13. Hubbert, C. et al. HDAC6 is a microtubule-associated deacetylase. *Nature* **417**, 455–458 (2002).
14. Akella, J. S. et al. MEC-17 is an alpha-tubulin acetyltransferase. *Nature* **467**, 218–222 (2010).
15. North, B. J., Marshall, B. L., Borra, M. T., Denu, J. M. & Verdin, E. The human Sir2 ortholog, SIRT2, is an NAD+-dependent tubulin deacetylase. *Mol. Cell* **11**, 437–444 (2003).
16. Szyk, A. et al. Molecular basis for age-dependent microtubule acetylation by tubulin acetyltransferase. *Cell* **157**, 1405–1415 (2014).
17. Skultetyova, L. et al. Human histone deacetylase 6 shows strong preference for tubulin dimers over assembled microtubules. *Sci. Rep.* **7**, 11547 (2017).
18. Hammond, J. W. et al. Posttranslational modifications of tubulin and the polarized transport of kinesin-1 in neurons. *Mol. Biol. Cell* **21**, 572–583 (2010).
19. Reed, N. A. et al. Microtubule acetylation promotes kinesin-1 binding and transport. *Curr. Biol.* **16**, 2166–2172 (2006).
20. Dompierre, J. P. et al. Histone deacetylase 6 inhibition compensates for the transport deficit in Huntington's disease by increasing tubulin acetylation. *J. Neurosci.* **27**, 3571–3583 (2007).
21. Li, L. et al. MEC-17 deficiency leads to reduced alpha-tubulin acetylation and impaired migration of cortical neurons. *J. Neurosci.* **32**, 12673–12683 (2012).
22. Dan, W. et al. Alpha-tubulin acetylation restricts axon overbranching by dampening microtubule plus-end dynamics in neurons. *Cereb. Cortex* **28**, 3332–3346 (2018).
23. Godena, V. K. et al. Increasing microtubule acetylation rescues axonal transport and locomotor deficits caused by LRRK2 Roc-COR domain mutations. *Nat. Commun.* **5**, 5245 (2014).
24. d'Ydewalle, C. et al. HDAC6 inhibitors reverse axonal loss in a mouse model of mutant HSPB1-induced Charcot-Marie-Tooth disease. *Nat. Med.* **17**, 968–974 (2011).
25. Park, I. Y. et al. Dual chromatin and cytoskeletal remodeling by SETD2. *Cell* **166**, 950–962 (2016).
26. Xie, X. et al. alpha-TubK40me3 is required for neuronal polarization and migration by promoting microtubule formation. *Nat. Commun.* **12**, 4113 (2021).
27. Zhang, D. et al. Metabolic regulation of gene expression by histone lactylation. *Nature* **574**, 575–580 (2019).
28. Li, L. et al. Glis1 facilitates induction of pluripotency via an epigenome-metabolome-epigenome signalling cascade. *Nat. Metab.* **2**, 882–892 (2020).
29. Zhang, N. et al. alpha-myosin heavy chain lactylation maintains sarcomeric structure and function and alleviates the development of heart failure. *Cell Res.* **33**, 679–698 (2023).
30. Yang, Z. et al. Lactylome analysis suggests lactylation-dependent mechanisms of metabolic adaptation in hepatocellular carcinoma. *Nat. Metab.* **5**, 61–79 (2023).

31. Varner, E. L. et al. Quantification of lactoyl-CoA (lactyl-CoA) by liquid chromatography mass spectrometry in mammalian cells and tissues. *Open Biol.* **10**, 200187 (2020).
32. Jia, M. et al. ULK1-mediated metabolic reprogramming regulates Vps34 lipid kinase activity by its lactylation. *Sci. Adv.* **9**, eadg4993 (2023).
33. Moreno-Yruela, C. et al. Class I histone deacetylases (HDAC1-3) are histone lysine delactylases. *Sci. Adv.* **8**, eabi6696 (2022).
34. Zu, H. et al. SIRT2 functions as a histone delactylase and inhibits the proliferation and migration of neuroblastoma cells. *Cell Discov.* **8**, 54 (2022).
35. Yang, K. et al. Lactate promotes macrophage HMGB1 lactylation, acetylation, and exosomal release in polymicrobial sepsis. *Cell Death Differ.* **29**, 133–146 (2022).
36. Mao, Y. et al. Hypoxia induces mitochondrial protein lactylation to limit oxidative phosphorylation. *Cell Res.* **34**, 13–30 (2024).
37. Gaffney, D. O. et al. Non-enzymatic lysine lactoylation of glycolytic enzymes. *Cell Chem. Biol.* **27**, 206–213 e206 (2020).
38. Pan, R. Y. et al. Positive feedback regulation of microglial glucose metabolism by histone H4 lysine 12 lactylation in Alzheimer's disease. *Cell Metab.* **34**, 634–648.e6 https://doi.org/10.1016/j.cmet.2022.02.013 (2022).
39. Wan, N. et al. Cyclic immonium ion of lactyllysine reveals widespread lactylation in the human proteome. *Nat. Methods* **19**, 854–864 (2022).
40. Walenta, S. et al. High lactate levels predict likelihood of metastases, tumor recurrence, and restricted patient survival in human cervical cancers. *Cancer Res.* **60**, 916–921 (2000).
41. Walenta, S. et al. Tissue gradients of energy metabolites mirror oxygen tension gradients in a rat mammary carcinoma model. *Int. J. Radiat. Oncol. Biol. Phys.* **51**, 840–848 (2001).
42. Quinn, W. J. et al. Lactate limits T cell proliferation via the NAD(H) redox state. *Cell Rep.* **33**, 108500 (2020).
43. Hu, J.X. et al. Macrophage migration inhibitory factor (MIF) acetylation protects neurons from ischemic injury. *Cell Death Dis.* **13**, 466 (2022).
44. Xiong, J. et al. Lactylation-driven METTL3-mediated RNA m(6)A modification promotes immunosuppression of tumor-infiltrating myeloid cells. *Mol. Cell* https://doi.org/10.1016/j.molcel.2022.02.033 (2022).
45. Izzo, L. T. & Wellen, K. E. Histone lactylation links metabolism and gene regulation. *Nature* **574**, 492–493 (2019).
46. Gonzalez-Rodriguez, P. et al. Disruption of mitochondrial complex I induces progressive parkinsonism. *Nature* **599**, 650–656 (2021).
47. Gudimchuk, N. B. & McIntosh, J. R. Regulation of microtubule dynamics, mechanics and function through the growing tip. *Nat. Rev. Mol. Cell Biol.* **22**, 777–795 (2021).
48. Akhmanova, A. & Kapitein, L. C. Mechanisms of microtubule organization in differentiated animal cells. *Nat. Rev. Mol. Cell Biol.* **23**, 541–558 (2022).
49. Shang, S., Liu, J. & Hua, F. Protein acylation: mechanisms, biological functions and therapeutic targets. *Signal Transduct. Target Ther.* **7**, 396 (2022).
50. Dancy, B. M. & Cole, P. A. Protein lysine acetylation by p300/CBP. *Chem. Rev.* **115**, 2419–2452 (2015).
51. Luo, M. Chemical and biochemical perspectives of protein lysine methylation. *Chem. Rev.* **118**, 6656–6705 (2018).
52. He, L. et al. C9orf72 functions in the nucleus to regulate DNA damage repair. *Cell Death Differ.* **30**, 716–730 (2023).
53. Li, L. et al. Enzymatic activity of the scaffold protein rapsyn for synapse formation. *Neuron* **92**, 1007–1019 (2016).
54. Yuan, L., Han, Y., Zhao, J., Zhang, Y. & Sun, Y. Recognition and cleavage mechanism of intron-containing pre-tRNA by human TSEN endonuclease complex. *Nat. Commun.* **14**, 6071 (2023).
55. Castoldi, M. & Popov, A. V. Purification of brain tubulin through two cycles of polymerization-depolymerization in a high-molarity buffer. *Protein Expr. Purif.* **32**, 83–88 (2003).

Acknowledgements

We thank X. Li, C. Fan, R. Wang and Z. Yang from the Molecular Imaging Core Facility (MICF); P. Hao, Z. Shi and C. Zhang from the Multi-Omics Core Facility (MOCF); and Y. Xiong, X. Ren, and J. Li from the Molecular and Cell Biology Core Facility (MCBCF); J. Wang from the Animal Core Facility at the School of Life Science and Technology, ShanghaiTech University for providing technical support. We thank Dr. Lei Diao and Dr. Lan Bao from CAS Center for Excellence in Molecular Cell Science, Dr. Zhen-Ge Luo, Dr. Fang Bai and Zhihao Gu from ShanghaiTech University for discussions and technical support. This study was supported by grants from the National Natural Science Foundation of China (91949117, 31871044 to L.L.), and the Lingang Laboratory (Grant No. LG-GG-202401-ADA060200 to L.L.).

Author contributions

L.L., S.S., and Z.X. designed the experiments and wrote the manuscript. S.S. and Z.X. performed and analyzed most of the experiments; L.H. performed and analyzed Mass spectrometry experiment. X.L. and Y.D.S. contributed to protein purification. Y.Y., Y.Z., S.L., X.Z., W.L., W.T., and Y.H.S. contributed to data analyses.

Competing interests

The authors declare no competing interests.

Additional information

Supplementary information The online version contains supplementary material available at https://doi.org/10.1038/s41467-024-52729-0.

Correspondence and requests for materials should be addressed to Lei Li.

Peer review information *Nature Communications* thanks Manuela Basso, and the other, anonymous, reviewer(s) for their contribution to the peer review of this work. A peer review file is available.